Earth Planet. Sci. Lett. 639 (2024) 118771

Contents lists available at ScienceDirect

Earth and Planetary Science Letters

journal homepage: www.elsevier.com/locate/epsl

The role of sulfate in the hydrothermal replacement of aragonite single crystals by calcite

Pablo Forjanes [a], José Manuel Astilleros [b,c,*], Lurdes Fernández-Díaz [b,c]

[a] GFZ German Research Center for Geosciences, Telegrafenberg, Potsdam 14473, Germany
[b] Departamento de Mineralogía y Petrología, Universidad Complutense, Madrid 28040, Spain
[c] Instituto de Geociencias (CSIC, UMC), Madrid 28040, Spain

ARTICLE INFO

Edited by: Prof A Jacobson

Keywords:
Aragonite
Calcite
$CaCO_3$
Sulfate
Mineral replacement reaction
Diagenesis

ABSTRACT

Aragonite ($CaCO_3$) is a stable calcium carbonate phase under high pressure conditions. However, its formation in (sub)surface environments, where calcite is the stable polymorph, is widespread. Regardless of its origin, aragonite is expected to undergo transformation into calcite under moderate pressures and temperatures. However, this transformation does not always take place, which results in the presence of abundant aragonitic relics in the geological record. Traditionally, this preservation has been explained by the presence of chemical inhibitors that prevent the conversion of aragonite to calcite. While it is widely accepted that magnesium (Mg) plays a key role in the polymorphic selection of $CaCO_3$, the influence of other ions has also been suggested. This work evaluates the effect that different concentrations of sulfate (SO_4^{2-}) in the fluid has on the progress of the aragonite-to-calcite transformation at 220 °C. Our results show that, upon reaction with deionized water or sulfate-poor solutions ($[SO_4^{2-}]_{aq} < 0.1$ mM), aragonite single crystals are extensively replaced by calcite aggregates (crystal size > 15 μm) through an interface coupled dissolution-precipitation reaction. The replacement starts at the aragonite crystal surfaces and advances inwards thanks to the development of an extensive network of fractures. Contrarily, when the solution bears higher concentrations of sulfate ($[SO_4^{2-}]_{aq} > 0.1$ mM), only a thin layer of smaller crystals of calcite (< 10 μm) form on the aragonite substrates, without any further transformation taking place. We interpret that these smaller crystals exert too little crystallization pressure and fail to promote the development of a network of fractures. In the absence of this network, the aragonite-calcite transformation cannot take place. The transformation does not occur neither when the experiments are conducted with deionized water and fragments of gypsum or anhydrite together with the aragonite grains. The results of this study shed light on the influence of dissolved sulfate in the kinetics of the fluid-driven transformation of aragonite into calcite. These results are useful to understand the preservation of aragonite in a variety of current geological settings and provide valuable insights for better understanding the diagenesis of sedimentary carbonates.

1. Introduction

Calcium carbonate ($CaCO_3$) mineral phases are widespread in Earth's surface and subsurface environments (Morse et al., 2007), notably as the main components of rocks like limestones and marbles. Although there are several $CaCO_3$ polymorphs, only calcite and aragonite are significant rock-forming minerals. The stability fields of calcite and aragonite have been well established for decades, with calcite being stable under ambient conditions and aragonite as a high-pressure phase (Carlson, 1983). Aragonite is indeed a common mineral in metamorphic rocks in blue-schist facies, where its preservation constitutes a useful indicator for calculating PT trajectories (Ernst, 1988). Interestingly, aragonite also forms extensively under subsurface pressure and temperature conditions, where calcite is the stable $CaCO_3$ polymorph. Aragonite is widely used by organisms to build their shells and skeletons, is a common abiogenic cement in sedimentary rocks, and is also a common phase in caves and soils (Frisia et al., 2002). Furthermore, most abiogenic limestones in present-day seas are aragonitic, a trend spanning much of the Phanerozoic (Hardie, 1996; Hashim and Kaczmarek, 2019). The precipitation of aragonite under calcite stability conditions has been attributed to many parameters, including supersaturation, pH, temperature, pressure, CO_2 content and, namely, the presence of

* Corresponding author at: Departamento de Mineralogía y Petrología, Universidad Complutense, Madrid 28040, Spain.
E-mail address: jmastill@ucm.es (J.M. Astilleros).

https://doi.org/10.1016/j.epsl.2024.118771
Received 3 November 2023; Received in revised form 3 April 2024; Accepted 13 May 2024
Available online 25 May 2024

impurities in the crystallization medium (primarily Mg) (Lippmann, 1973; Fernandez-Diaz et al., 1996; Nielsen et al., 2013; Sun et al., 2015)

Irrespective of aragonite's origin, this phase should eventually convert to calcite under (sub)surface conditions. The transformation is rapid when the presence of a fluid facilitates that it occurs through a dissolution-crystallization mechanism (Perdikouri et al., 2011). Contrarily, it is sluggish, even for geological standards, under dry conditions, more so at the low temperature's characteristics of Earth's upper crust (Brown et al., 1962). The geologic record hosts a plethora of aragonite-rich ancient rocks and fossils where the aragonite-calcite transformation hasn't occurred at all or where aragonite persists as relics inside calcite bodies. Some examples include Jurassic aragonitic bivalves' shells (Sandberg and Hudson, 1983), Cretaceous aragonitic turtle eggshells (Choi et al., 2022) as well as the Triassic aragonite columnar crystals associated to Keuper sediments in the Iberian Range (Spain), where this mineral was first described (Herrero et al., 2020).

Multiple studies have concluded that the same ions that promote the formation of aragonite can also prevent its later transformation to calcite (Bischoff and Fyfe, 1968). It is widely accepted that magnesium, the most common divalent cation in seawater, influences the crystallization and growth of calcium carbonate, inhibiting calcite crystal growth. This, in turn, fosters the formation of metastable aragonite and retards its transformation to calcite (Bischoff and Fyfe, 1968; Katz, 1973; Fernandez-Diaz et al., 1996; Hashim and Kaczmarek, 2021; Turchyn et al., 2021). This role has been attributed to the inhibitory effect that dissolved magnesium has on the growth of calcite (Astilleros et al., 2010; Sun et al., 2015). Similarly, some works have drawn attention to the influence that some anionic groups, namely sulfate and phosphate, have in the polymorphic selection of $CaCO_3$, also by inhibiting the formation of calcite (Mucci, 1986; Staudt et al., 1994; Fernández-Díaz et al., 2010). Even though sulfate is, after Cl, the second most abundant anion in seawater (Algeo et al., 2015) as well as a main component of marine sediments and evaporites, its relevance in the polymorphic selection of $CaCO_3$ and in the preservation of metastable polymorphs is still a major subject of debate. Many authors attribute the metastable formation of aragonite in various geological settings solely to the influence of the magnesium present in the crystallization medium, but a combined influence of magnesium and sulfate resulting in a synergistic effect has also been proposed (Davis et al., 2000; Bots et al., 2011; Nielsen et al., 2016; Boon et al., 2020; Goetschl et al., 2019). Most of the works on the influence of sulfate have focused on its role in the formation and evolution of $CaCO_3$ precipitates (Fernández-Díaz et al., 2010; Cuesta Mayorga et al., 2019). To our knowledge, no study has addressed the influence of dissolved sulfate in the fluid-driven transformation of aragonite single crystals into calcite. This work aims to fill this void and has three main goals: (i) determining whether dissolved sulfate inhibits the replacement of aragonite single crystals by calcite and, if so, (ii) to what extent and (iii) through which mechanism. To reach these goals, we have conducted experiments of interaction between millimetric aragonite single crystals and aqueous solutions bearing different sulfate concentrations, under hydrothermal conditions. We discuss this influence taking both thermodynamic and kinetics factors into consideration. Moreover, we draw conclusions on the implications of our results regarding calcium carbonate diagenesis and, particularly, the preservation of aragonite relicts in sedimentary rocks.

2. Materials and methods

We conducted interaction experiments using aragonite single crystals. Aragonite samples were 10–20 cm crystals collected in the Triassic Keuper sediments of the Iberian Belt (Minglanilla, Castilla - La Mancha, north-eastern Spain) in spring 2018. We cut the crystals using a diamond saw into ≈ 4 × 4 × 2 mm fragments parallel to the $(001)_{Arg}$-face and washed them with deionized water (MiliQ) before the experiments. Polished cross sections of the starting material showed no cracks nor pores in back-scattered electron microscope images (Fig. 1).

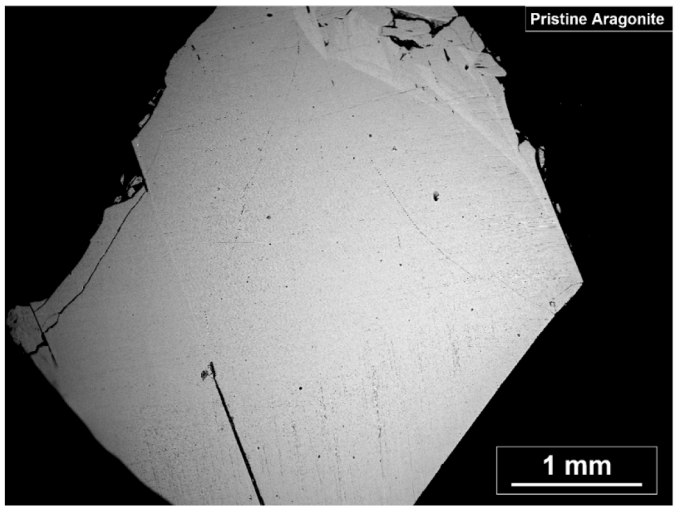

Fig. 1. BSE image of a polished cross section of an unreacted aragonite single crystal. The crystal shows no fractures nor porosity.

The interaction experiments were conducted using solutions bearing different concentrations of SO_4^{2-} (Systems A1 to A9; Table 1; Table A1). The aqueous solutions were prepared dissolving reagent grade Na_2SO_4 (Sigma Aldrich, Reagent Grade < 99.0%) in high purity deionized water (miliQ water, 18 MΩ·cm). Sulfate concentrations between 0 and 30 mM SO_4^{2-} were used, being the maximum concentration similar to that of modern-day seawater (≈ 29 mM; Algeo et al., 2015). Interaction experiments between aragonite single crystals and deionised water (miliQ) were also performed to observe the behaviour of the crystals in a SO_4^{2-}-free system (System A0). For the sake of consistency with recent experimental studies of the hydrothermal alteration of aragonite (Perdikouri et al., 2011; Casella et al., 2017; Forjanes et al., 2022), in each experimental run conducted in this work, 3 aragonite crystals were placed into a polytetrafluoroethylene (PTFE) vessel together with 10 mL of the aqueous solution (Table 1). The PTFE vessel was then sealed with a PTFE cover and inserted into a stainless -steel autoclave, which was subsequently sealed, and kept in an oven at 220 °C for times in the range between 1 and 30 days (Table 1 *and* Table A1). The pressure was not independently controlled and corresponded solely to the vapour pressure at the given temperature (approx. 2000 kPa). After the termination of the experiments, the autoclaves were recovered from the oven, cooled down at room temperature (20 °C) and opened. The recovered samples were washed with miliQ water and dried overnight at 40 °C in a furnace before being prepared for further analysis.

The first interacted aragonite fragment was analysed by Fourier Transform Infrared (FTIR) spectroscopy using a FTIR ThermoFisher Nicolet iS5 spectrometer equipped with an iD7 diamond detector and a

Table 1
Experimental conditions of the hydrothermal experiments.

System Name	*Solution Composition*	*Experimental Length*
Experiments using abiogenic single crystals (3 aragonite single crystals + 10 mL of aqueous solution)		
A0–1 to A0–5	*Deionised water (miliQ)*	*1 day (−1)*
A1–1 to A1–5	*0.005 mM* SO_4^{2-}	*3 days (−2)*
A2–1 to A2–5	*0.01 mM* SO_4^{2-}	*7 days (−3)*
A3–1 to A3–5	*0.05 mM* SO_4^{2-}	*14 days (−4)*
A4–1 to A4–5	*0.1 mM* SO_4^{2-}	*30 days (−5)*
A5–1 to A5–5	*0.5 mM* SO_4^{2-}	
A6–1 to A6–5	*1 mM* SO_4^{2-}	
A7–1 to A7–5	*5 mM* SO_4^{2-}	
A8–1 to A8–5	*10 mM* SO_4^{2-}	
A9–1 to A9–5	*30 mM* SO_4^{2-} (≈ seawater)	
A10–1 to A10–5	*miliQ water + 3 anhydrite fragments*	
A11–1 to A11–5	*miliQ water + 3 gypsum fragments*	

diamond attenuated total reflectance (ATR) accessory. FTIR spectra were recorded on the surfaces of the altered samples in the 1600–550 cm^{-1} range by the coaddition of 64 scans. These aragonite samples were then crushed using an agate mortar and analysed with powder X-ray diffraction (pXRD) for phase composition evaluation. The diffractometers were a Bruker D8-Advance or a STOE StadiP devices using Cu-Kα radiation (Bragg-Bentano geometry), and a scan recording in the 2θ angle range between 20° and 50° Standard mineral files of the American Mineralogist Crystal Structure Database and diffraction diagrams were correlated to determine solid phases. The relative abundances of aragonite and calcite were determined using the ratio of the aragonite 111 and calcite 104 peaks using the CrystalDiffract 6.0 Software. This was done by comparing the diffraction patterns of the samples to that of an artificial mixture created with the CIFs of calcite (Markgraf and Reeder, 1985) and aragonite (De Villiers, 1971). The second interacted aragonite fragment was mounted on a holder and coated with gold (Quorum Q150R-S; 15 nm). The third aragonite fragment was inserted in a silicon mould with the (001) face parallel to the mould base, embedded in epoxy resin (ResinPro) and polished down to the middle using 4 grinding steps (P180; P320; P600 and P1200, respectively). This sample was later coated with carbon (QuorumQ15OT-E; 8 nm). Whole and epoxy embedded samples were imaged using a scanning electron microscope (SEM) (JEOL JSM 6400, Akishima, Tokyo, Japan; 40 kV). The progress of the replacement reaction in the polished sections was followed by observing contrast differences in electron backscattered (BSE) images, with calcite appearing darker and aragonite appearing brighter. Average crystal size of the overgrowing crystals was determined analysing SEM images with the ImageJ software.

Aiming to better understand the behaviour of aragonite crystals in sediments where the dissolution of sulfate bearing minerals is the eventual source of sulfate, additional experiments were carried out. In these experiments, 3 fragments of anhydrite ($CaSO_4$; Naica, Mexico) (System A10) or gypsum ($CaSO_4 \cdot 2H_2O$; Teruel Spain) (System A11) single crystals were introduced into the PTFE vessels together with the 3 aragonite crystals and 10 ml of deionised (miliQ) water (Table 1; Table A1). The characterisation of the altered aragonite, anhydrite and gypsum fragments was performed in the same way as described above. Nevertheless, the diffractograms of the altered samples of systems A11

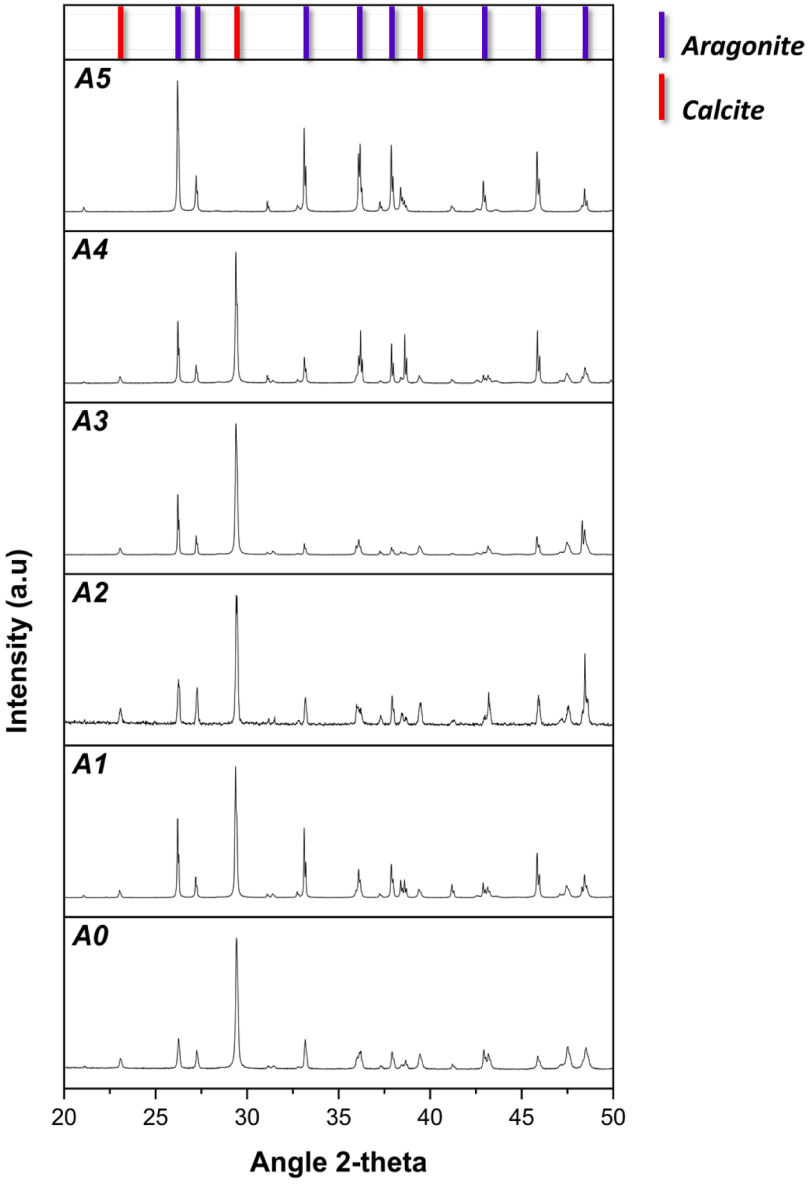

Fig. 2. Selected pXRD diffractograms of aragonite single crystals after 30 days interaction with aqueous solutions bearing different concentrations of sulfate. Aragonite is only partially replaced by calcite when $[SO_4^{2-}]_{aq} < 0.5$ mM (system A5).

and A12 were collected between 10 and 50° to avoid missing the possible appearance of the (010) peak of gypsum.

3. Results

After the interaction, the reacted aragonite crystals undergo striking changes in their colour. The samples interacting with fluids with the lower concentrations of sulfate or deionized water appear completely white after the interaction. Contrarily, samples interacting with solutions with $[SO_4^{2-}]_{aq} \geq 0.5$ mM are virtually indistinguishable from the pristine aragonite crystals (Fig. A1). pXRD analysis of altered aragonite samples show that the crystals which interact with miliQ water or solutions with low concentrations of sulfate (System A0-A4) consist of calcite and aragonite. Contrarily, samples reacting with fluids with $[SO_4^{2-}]_{aq} \geq 0.5$ mM, only show peaks corresponding to aragonite (Fig. 2 *and* Table A1). In those systems where aragonite transforms into calcite, this process takes place at a slower rate the higher the sulfate concentration is in the solution. Thus, samples altered for 3 days in systems A0 and A1 contain above 10 wt.% calcite. Reaching a similar degree of aragonite-to-calcite transformation requires 7 days in system A2, 14 days in system A3 and 30 days in system A4. After 30 days, the amount of calcite in altered samples in systems A1-A4 approaches 40 wt.% (Fig. A2).

Similarly, when the aragonite grains react with miliQ water together with 3 fragments of anhydrite or gypsum there is almost no transformation of the aragonite grains to calcite (Fig. 3). Simultaneously, the anhydrite fragments remain unaltered and do not undergo any mineralogical transformation, while the gypsum fragments undergo a complete transformation into anhydrite (Fig. 3).

Epoxy-embedded polished sections in Fig. 4 correspond to aragonite crystals after 30 days interaction with aqueous solutions bearing $[SO_4^{2-}]_{aq}$ between 0.005 and 0.05 mM. As can be seen, the reacted samples appear extensively fractured and consist of two mineral phases clearly distinguishable by their different brightness in BSE images. The darker phase is calcite, while the lighter one is aragonite. Two types of calcite crystals can be distinguished: (i) euhedral crystals that appear building up an overgrowth surrounding the original aragonite (blue triangles in Fig. 4) and (ii) crystals that grow within the fractures that cross the altered sample (yellow circles in Fig. 4). Aragonite relicts appear separated from each other by calcite grown within the fractures (green stars in Fig. 4). Within calcite regions formed abutting fractures, aragonite relicts can also be observed (white arrows in Fig. 4*b*). Similar features are observed in aragonite single crystals after interaction with deionized water (Fig. A3).

The outcome of the interaction is slightly different when the sulfate concentration in the aqueous solution is 0.1 mM (System A4; Fig. 5). After 30 days interaction, the aragonite crystal appears widely fractured and surrounded by a 150–200 μm-thick calcite overgrowth (blue triangle in Fig. 5). However, little calcite forms associated with the fractures. When the sulfate concentration is ≥ 0.5 mM (Systems A5 to A9; Fig. A4)

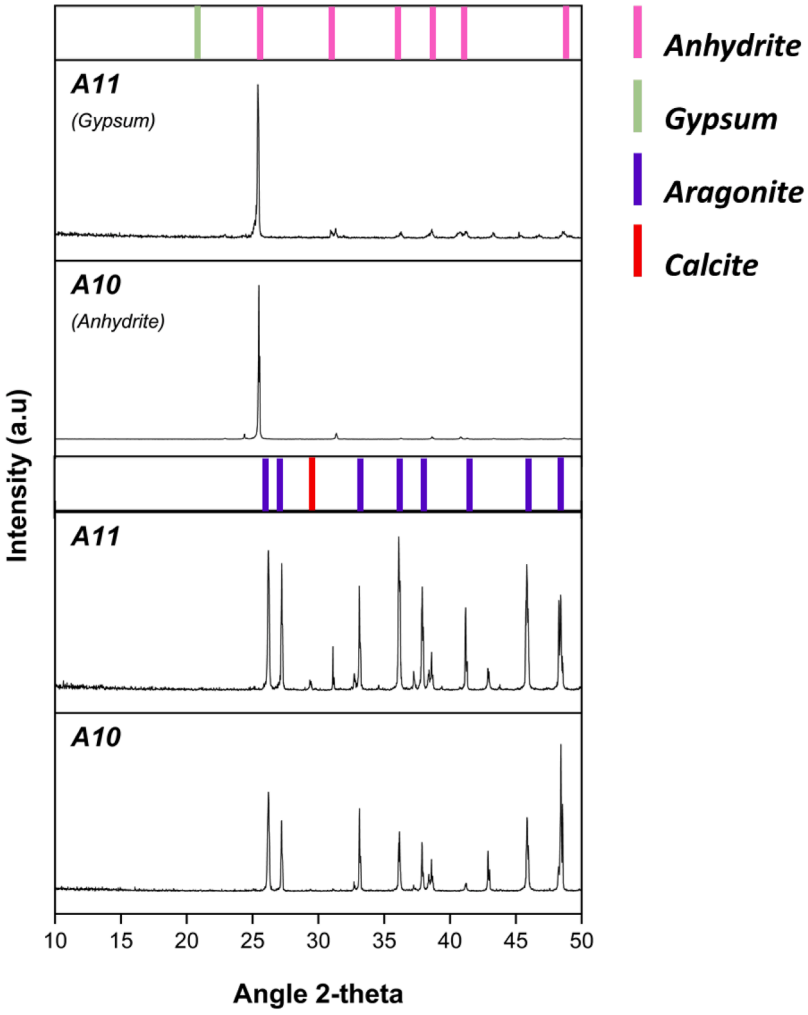

Fig. 3. pXRD diffractograms of aragonite single crystals after 30 days interaction with miliQ water and 3 fragments of anhydrite or gypsum. Aragonite is only slightly transformed into calcite when it reacts with gypsum grains. When it does so with anhydrite fragments all the peaks in the diffractogram of the altered crystals correspond to aragonite. Anhydrite does not undergo any transformation during the interaction while gypsum fully transforms into anhydrite.

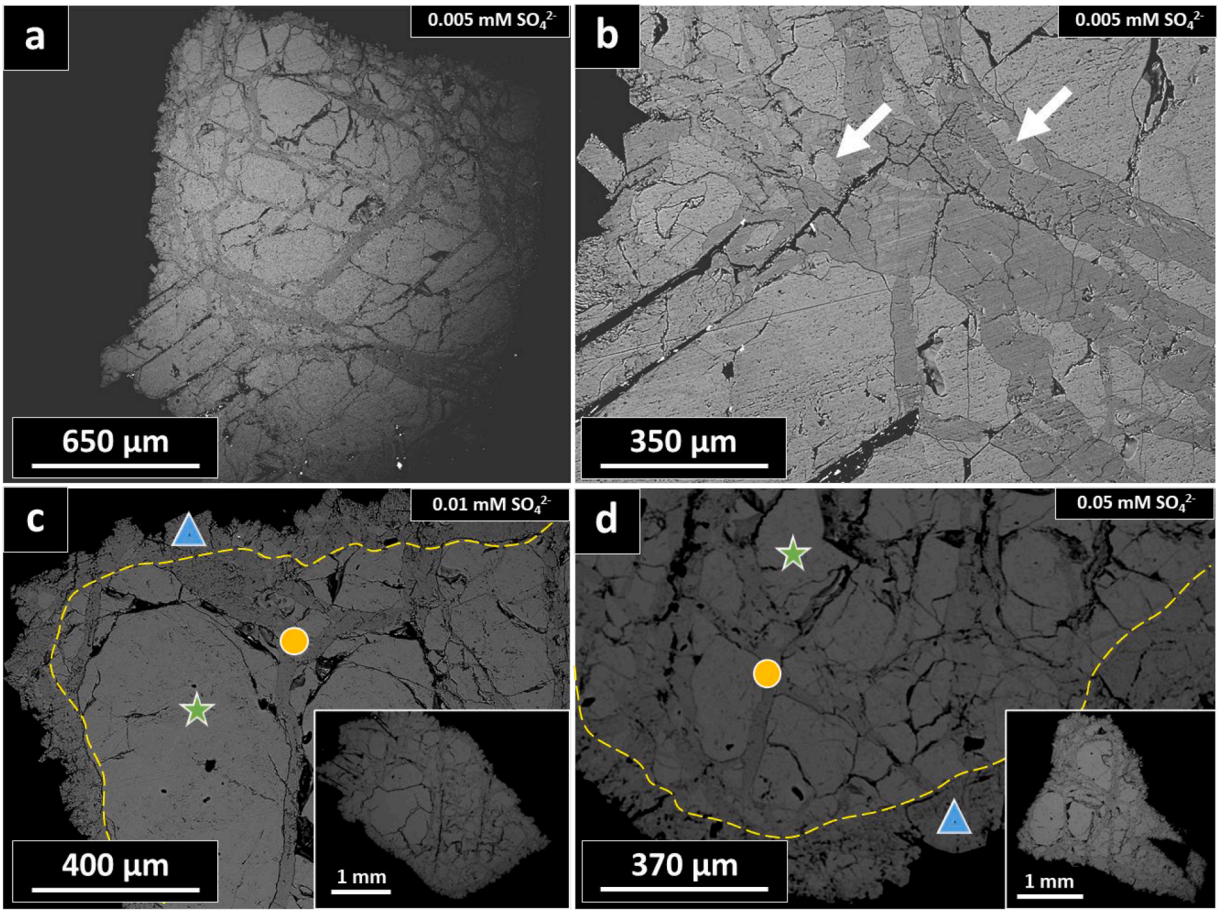

Fig. 4. BSE images of cross sections of aragonite samples treated with aqueous solutions bearing low concentrations of sulfate ($[SO_4^{2-}]_{aq} \leq 0.05$ mM) during 30 days at 220 °C. The interaction leads to an extensive replacement of the aragonite grains (green star; bright mineral) by calcite (dark mineral) through the fracturing of the aragonite parent mineral. Calcite grows both as (i) overgrowths (blue triangles) surrounding the original aragonite crystal and (b) as crystals filling the fractures (yellow circles). The yellow line has been drawn to separate the overgrowth from the original aragonite crystal.

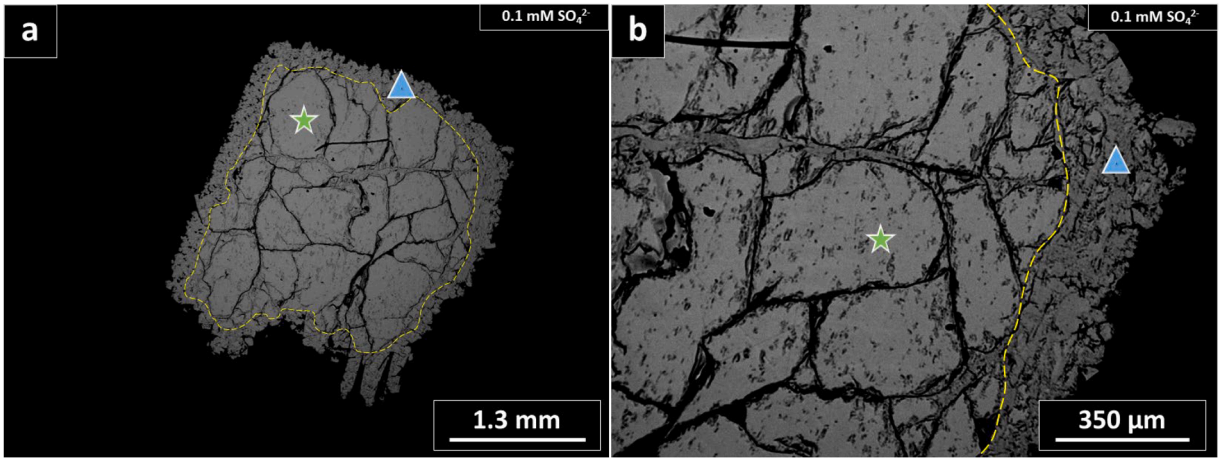

Fig. 5. BSE images of a cross section of an aragonite crystal treated with a $[SO_4^{2-}]_{aq} = 0.1$ mM aqueous solution during 30 days at 220 °C. Similarly to what happened after interaction with solutions with lower sulfate concentrations, an overgrowth of calcite (blue triangle) surrounds the aragonite crystal (green star). Interestingly, the fractures are barely filled with calcite.

the aragonite crystals remain unaltered, with no distinguishable overgrowths nor fractures, and are virtually indistinguishable from the pristine samples (Fig. 1).

When the aragonite fragments react with miliQ water and the sulfate minerals (gypsum or anhydrite; Systems A10 and A11), they also remain unaltered, with no evidence of fracture nor overgrowth formation (Fig. A5). SEM imaging of cross sections of the anhydrite crystals after the interaction don't show any replacement taking place (Fig. A6). Polished-sections of the altered gypsum fragments were not prepared due their extreme fragility after their transformation in anhydrite had

taken place. These samples disintegrated into fragments smaller than 0.1 mm as they were handled (Fig. 3).

The surfaces of the hydrothermally altered aragonite crystals were imaged with SEM. The interaction of the aragonite fragments with fluids bearing different amounts of sulfate leads to the formation of calcite crystals growing on the aragonite surfaces regardless of the initial sulfate concentration in the fluid (Figs. 6, 7 *and A7*). However, the size and morphology of the so-formed crystals vary dramatically depending on the initial composition of the aqueous solution (Figs. A8 and A9*)*. Thus, aragonite crystals reacted with solution A1 appear completely carpeted by rhombohedron-shaped calcite crystals. The newly formed crystals have average sizes larger than 20 μm, as measured in SEM images with ImageJ, with those formed at the edges of the aragonite faces reaching sizes of several hundred microns (white arrows in Fig. 6b*;* the yellow line marks the boundary of the aragonite (001) face). The overgrowing calcite crystals appear completely carpeting the surfaces of the aragonite grains forming replaced layers traversed by numerous fractures (white arrows Fig. 6*c*). Contrarily, calcite crystals grown in solutions with higher sulfate concentrations show increasingly prismatic and elongated habits. Furthermore, the carpeting is not complete anymore for $[SO_4^{2-}]_{aq} \geq 0.5$ mM and the size of the crystals plummets to less than 10 μm (Figs. A8 and A9). For the highest sulfate concentrations used in this work (10 and 30 mM), aragonite dissolution marks can be observed together with few small calcite crystals growing around (Fig. 7).

The interaction of aragonite fragments with miliQ water and gypsum or anhydrite fragments results in only a very slight alteration of the original surfaces, characterized by the development of dissolution marks and the formation of scarce calcite patches consisting of 5–10 μm-sized crystals (Fig. A10).

The surface of the altered products was further studied by infrared spectroscopy. The collected IR spectra show absorbence bands characteristic of calcite and/or aragonite (Vagenas et al., 2003; Toffolo et al., 2019). Fig. 8 shows the relevant region of the IR spectra of aragonite crystals after 30 days interaction with aqueous solutions A0, A2, A4 and A6. All spectra show strong absorption bands in the ranges 1400–1500 cm^{-1} (v_3), 1070–1100 cm^{-1} (v_1), 850–900 (v_2) and 700–720 (v_4), reflecting the internal CO_3^{2-} vibrations that can be attributed to calcite and/or aragonite.

Interestingly, the spectra of samples A2 and A4 show small bulges that do not appear in the spectra of the sample interacted with deionized water (System A0; Fig. 9). These wavelengths fit well with those corresponding to the v_4 antisymmetric bending vibrations (580–670 cm^{-1}; Fig. 9a-d) and the v_3 antiysmmetric stretch vibrations (around 1030 and 1180 cm^{-1}; Fig. 9e-h) of the sulfate tetrahedra in minerals (Ross, 1974). These bulges are not distinguishable anymore in the spectra of samples interacted with aqueous solutions containing higher sulfate concentrations ≥ 0.5 mM.

4. Discussion

4.1. The fluid-driven replacement of aragonite single crystals by calcite

Our results show that aragonite fragments undergo significant transformation into calcite (up to 50 wt.%) when exposed to aqueous

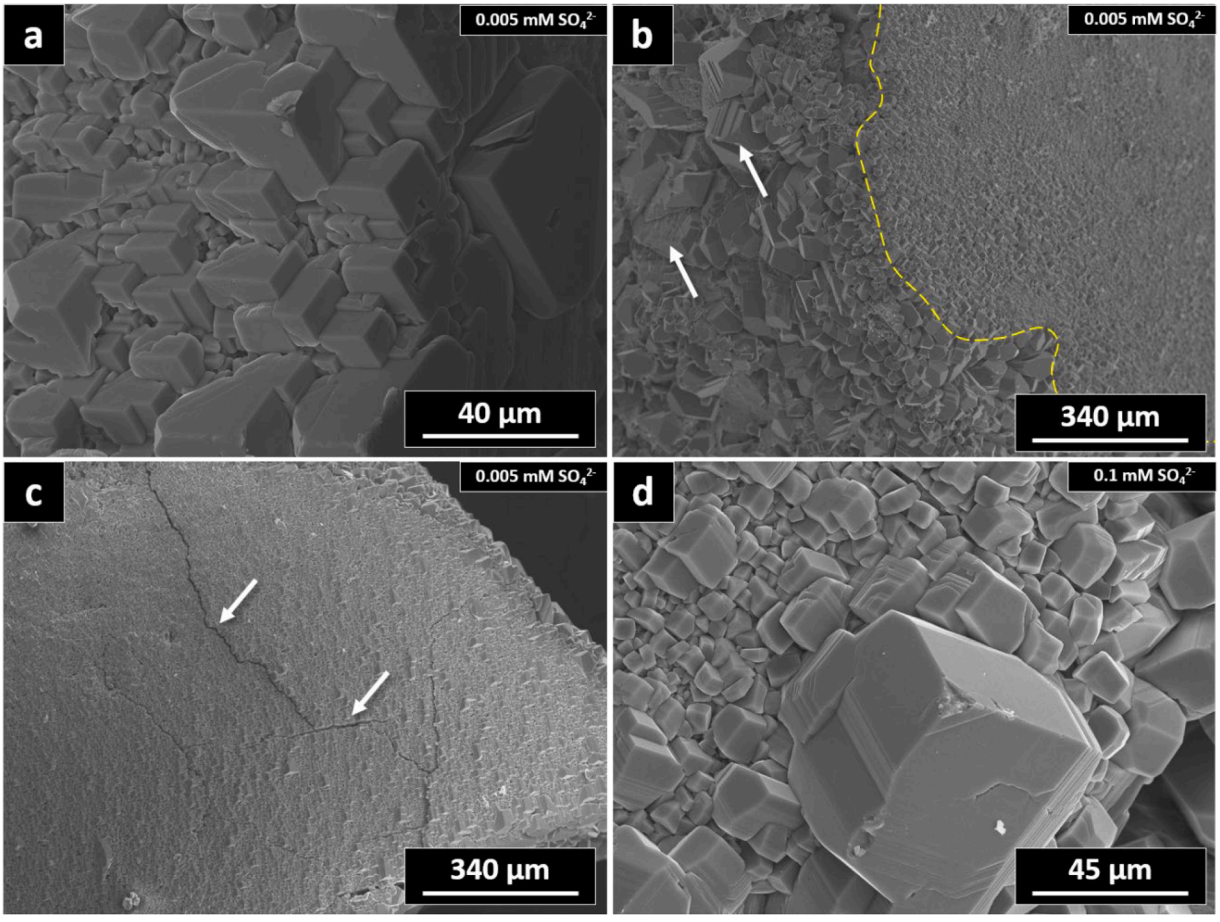

Fig. 6. SEM micrographs showing calcite crystals growing on the aragonite (001) surfaces after 30 days interaction between the aragonite grains and fluids with different concentrations of sulfate. The interaction leads to the formation of calcite crystals on the aragonite substrates regardless the sulfate concentration in the aqueous solution. However, sulfate concentration has a big impact in the morphology, abundance, and size of the newly formed calcite crystals. Low concentrations of sulfate lead to the development of big, rhombohedral crystals that rapidly cover the aragonite substrates.

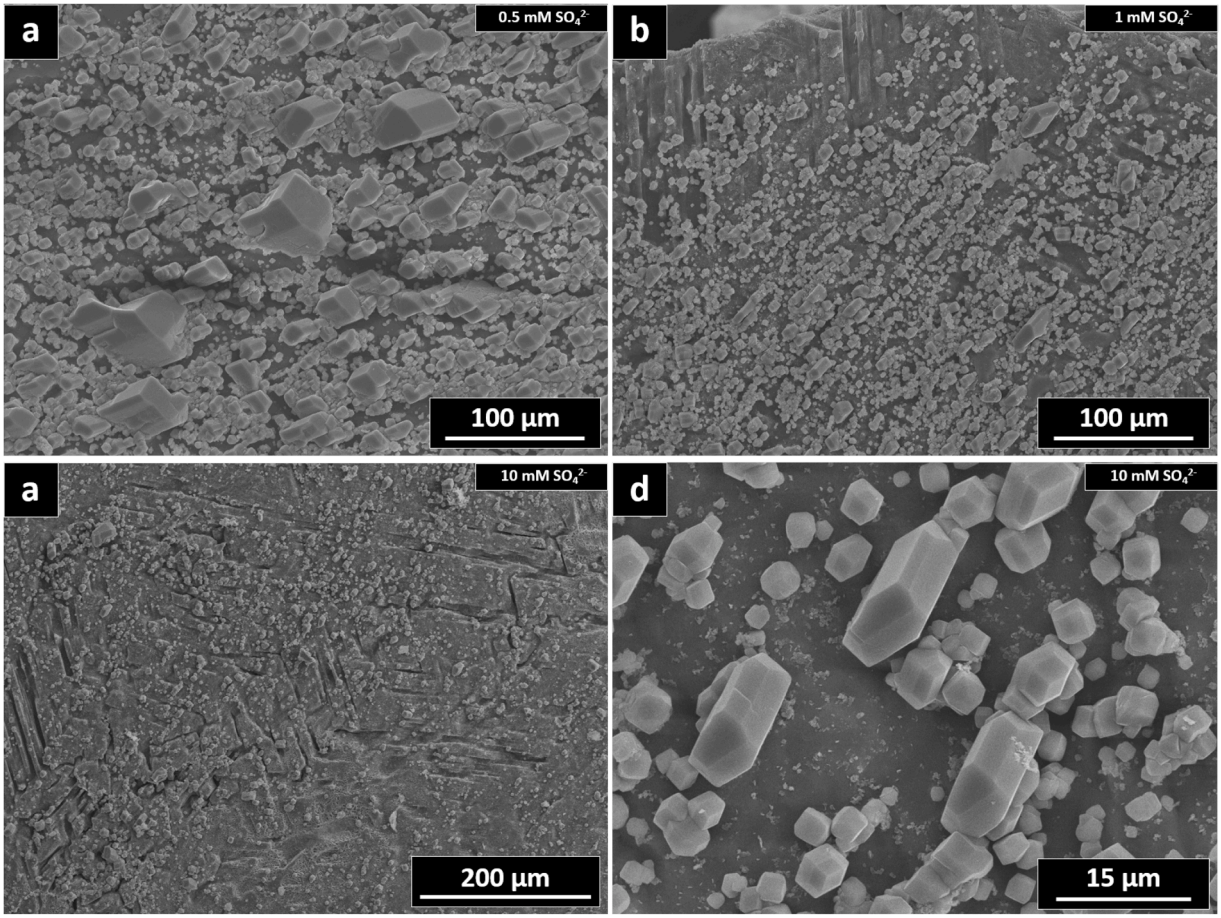

Fig. 7. SEM micrographs showing calcite crystals growing on the aragonite (001) surfaces after 30 days interaction between the aragonite grains and fluids with different concentrations of sulfate. When the fluid bears high concentrations of sulfate, the formation of small and prismatic crystals of calcite is observed. These crystals fail to fully carpeting the aragonite substrate.

solutions with low concentrations of sulfate ($[SO_4^{2-}]_{aq} < 0.1$ mM). The replacement reaction begins in the outermost parts of the fragments and progresses inwards through the fractures formed during the transformation, defining a sharp and irregular reaction front roughly parallel to the original aragonite surface. Throughout the transformation, the external size and shape of the original aragonite fragments are preserved, leading to the formation of pseudomorphs. These characteristics of the aragonite-by-calcite replacement are indicative of the process occurring via an interface coupled dissolution-precipitation (ICDP) mechanism. The same conclusion was reached by Perdikouri et al. (2011), who investigated the hydrothermal transformation of aragonite single crystals into calcite aggregates after interaction with deionized water as well as fluids bearing Ca^{2+} and CO_3^{2-} ions.

Upon interaction with the solution, the aragonite fragments undergo dissolution, releasing CO_3^{2-} and Ca^{2+} ions into the fluid. At some point the fluid reaches supersaturation with respect to calcite, leading to the precipitation of this mineral on the parent aragonite surfaces, forming an overgrowth. The precipitation of calcite results in a depletion of the solution reagents which, in turn trigger further dissolution of the parent aragonite. This establishes a feedback loop between aragonite dissolution and calcite precipitation, a phenomenon well-documented in the literature (Putnis, 2009; Ruiz-Agudo et al., 2014; Putnis and Putnis, 2022). The conversion of the aragonite grains into calcite begins with the formation of 3D calcite nuclei on the aragonite substrate. The growth and coalescence of these 3D nuclei lead to the complete carpeting of the parent surfaces. The 3D nature of the overgrowth determines that the nanotopographic features of the aragonite original surfaces are lost and the microtopographic ones are only roughly preserved, which is not unusual during ICDP reactions that are poorly coupled and/or involve a positive molar volume change, as is the case of the aragonite-calcite transformation ($\Delta v = +8.44\%$) (Qian et al., 2010, 2011; Perdikouri et al., 2011; Zhao et al., 2014). After the full carpeting of the aragonite parent surfaces, a continuous communication between the bulk fluid and the primary phase-secondary phase interface has to develop for the reaction to progress. In ICDP reactions, this communication is often provided by the formation of interconnected porosity within the secondary layer during the transformation. This porosity commonly forms to balance negative changes in molar volume and/or solubility between both phases (Putnis, 2009; Ruiz-Agudo et al., 2014). Because the molar volume change in this transformation is not negative and the solubility change is small ($K_{sp\ calcite} = 10^{-11.80}$ and $K_{sp\ aragonite} = 10^{-11.74}$ at 220 °C; Plummer and Busenberg, 1982) no interconnected porosity emerges during the transformation of aragonite into calcite. In the absence of porosity, ICDP reactions can still progress if a network of fractures develops, dividing the parent mineral into independent domains (Ruiz-Agudo et al., 2014). The formation of such a network was, indeed, observed in the work of Perdikouri et al. (2011). We also observe the formation of such fractures in our experiments, but only when aragonite crystals interact with solutions containing $[SO_4^{2-}]_{aq} < 0.5$ mM. A fracture network can also provide the necessary pathway for the fluid to reach the primary phase-secondary phase interphase. Fracturing of the parent crystal is triggered by the pressure exerted by the crystallization of the secondary phase. Therefore, as new fresh aragonite surfaces are exposed to interaction with the fluid in fractures, new calcite crystals can form on these surfaces, promoting more fracturing and thereby facilitating the progress of the ICDP reaction. Previous works have

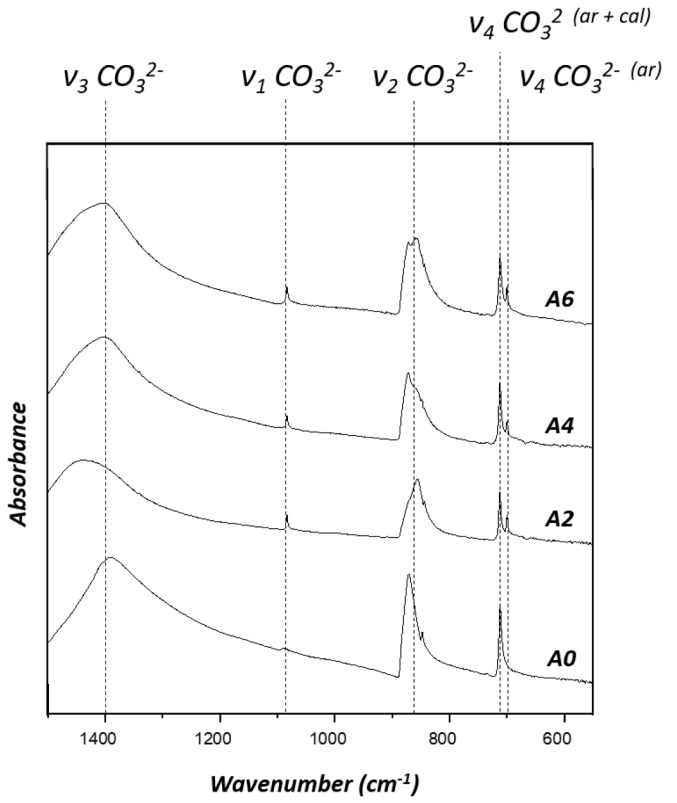

Fig. 8. FTIR spectra of the aragonite reacted samples after 30 days of interaction in the case of the experiments A0 ($[SO_4^{2-}]_{aq}$ = 0 mM), A2 ($[SO_4^{2-}]_{aq}$ = 0.01 mM), A4 ($[SO_4^{2-}]_{aq}$ = 0.1 mM) and A6 ($[SO_4^{2-}]_{aq}$ = 1 mM). All the spectra are characterized by strong bands in the 1400–1500 cm^{-1} (v_3), 1070–1100 cm^{-1} (v_1), 850–900 cm^{-1} (v_2) and 700–720 cm^{-1} (v_4), which are characteristics of the carbonate ion vibrational modes in aragonite and/or calcite: 1420 (v_3), 875 (v_2) and 713 (v_4) in calcite and 1475 (v_3), 1083 (v_1), 856 (v_2) and 713 + 700 (v_4) in aragonite (Vagenas et al., 2003; Toffolo et al., 2019).

shown that the heterogeneous nucleation of calcite on aragonite surfaces primarily occurs at defect sites on the substrate, like dislocation outcrops, subgrain and twin boundaries or cracks, where surface energy is higher (De Yoreo and Vekilov, 2003). The stress exerted by growing calcite crystals concentrates in these sites, promoting the fracturing of the substrate (Plümper et al., 2012). This stress, which can be described as equivalent to the crystallization pressure (Δp) is defined by the Eq. (1) (Scherer, 1999; Steiger, 2005):

$$\Delta p = \frac{nRT}{Vm} \ln \frac{IAP}{k_{sp}} \quad (1)$$

In this equation n represents the number of molecules per unit cell in the solid phase, R is the gas constant, T is the temperature, IAP is the ion activity product, K_{sp} the solubility product of the growing phase (IAP/k_{sp} is the supersaturation, β) and Vm is the molar volume. This equation highlights that there is a direct relationship between crystallization pressure and supersaturation (Schiro et al., 2012). Consequently, a crystal growing within a confined material can only generate stress upon contact with supersaturated solutions. The stress required for a subcritical fracture to open at a pre-existing dissolution pit or crack can be estimated using the approach followed by Monasterio-Guillot et al. (2021). Jacobsen et al., (2015) demonstrated that a fracture can open perpendicularly to that fracture plane when:

$$\sigma_c = \frac{K_{Ic}}{1.156\sqrt{c}} \quad (2)$$

where K_{Ic} is the fracture toughness of the material and c is the radius of the pre-existing fracture. The published K_{Ic} values for aragonite single crystals vary within a large range and, above all, are extremely dependant on the crystallographic face considered. However, in the case of aragonite (001) face, which is the one this work is focused on, a K_{Ic} around 0.3 MPa/m^2 has been commonly agreed on (Lew et al., 2023). Using this K_{Ic} value and an average fracture radius of 10, 20 or 40 μm, the equation proposed by Jacobsen et al. (2015) yields values of 85 MPa, 58 MPa and 42 MPa, respectively. These would be the critical values necessary for new fractures to open in aragonite crystals, this is, calcite crystals growing within dissolution pits or pre-existing cracks would have to exert Δp values higher than the listed values. These calculations evidence that the smaller a fracture is, the more stress the growing crystal has to exert to open it. It should be noted that the theoretical maximum value of the tensile strength for a crystal is $E/10$ (E being the Young modulus of aragonite = 99.5 GPa; (Katti and Katti, 2001) i.e. 9.5 GPa for aragonite, but that the real value is usually much lower due to the presence of crack-like defects on or within the crystal (Idrissi et al., 2016). This explains why fracturing of aragonite is usually observed under much lower σ_c values. In fact, numerous experimental studies have shown that aragonite (biogenic and abiogenic) can fracture under tensile strengths as low as 100 or even 10 MPa (Meyers et al., 2008); which are in the same range as those calculated above. Incorporating the calculated σ_c values into Eq. (1), it yields the following supersaturations with respect to calcite required for widening the aforementioned fractures: $\beta_{c=40} = 1.13$, $\beta_{c=20} = 1.20$ and $\beta_{c=10} = 1.28$. ICDP reactions take place due to the existence of a disequilibrium between the fluid and the parent solid phase. This drives the dissolution of the latter until the fluid reaches saturation ($\beta = 0$). In the case under consideration, when this situation is reached at the thin boundary layer of fluid in contact with the aragonite surface, the system is also supersaturated with respect to calcite. At this stage, calcite can precipitate. Since the coupling between the rates of aragonite dissolution and calcite precipitation is fairly good, it can be assumed that the supersaturation of this thin layer of fluid at the aragonite-calcite interface will be close to the ratio between the solubility products of these two phases at the experimental temperature (T = 220 °C; K_{sp} calcite = $10^{-11.80}$ and K_{sp} aragonite = $10^{-11.74}$ at 220 °C), this is, $\beta = 1.14$. Note that this supersaturation is very similar to that required according Eq. (1) to generate a stress high enough to widen a 40-μm fracture (42 MPa). Once fractures emerge, they can widen and propagate via further calcite crystallization within the fractures. This sequence ultimately gives rise to the generation of new fractures, which eventually ends in the formation of a hierarchical fracture network (Putnis and Putnis, 2007; Røyne et al., 2008; Jamtveit et al., 2009). ICDP reactions where formation and widening of fractures have been observed include the carbonation of pyroxenes (Monasterio-Guillot et al., 2021) and olivine (Lafay et al., 2018) or the conversion of aragonite into otavite (Julia et al., 2023), amongst others.

Interestingly, despite the formation of an extensive network of fractures, a complete replacement of the aragonite parent material is not observed under any of the experimental conditions considered in this work. Thus, even under those conditions that allow the highest degree of aragonite transformation into calcite, numerous aragonite relicts remain unaltered after 30 days interaction (Fig. 4). Similar results were reported by Perdikouri et al. (2011), who never observed a complete replacement of aragonite by calcite regardless of the composition of the fluid. Sandberg and Hudson (1983) studied Jurassic bivalve shells, originally aragonitic, in which the extensive replacement of the aragonitic microstructure by calcite had not prevented numerous relicts of the original microstructure to survive the transformation. These aragonitic relicts appeared surrounded by a mosaic of large, neoformed crystals of low magnesian calcite (LMC). Similarly, Casella et al. (2018) studied the alteration of various aragonitic exoskeletons in contact with diagenetic-mimicking fluids. These authors observed a sequential process where the syntaxial growth of abiogenic aragonite preceded the formation of small patches of high magnesium calcite (HMC). These HMC crystals were finally replaced by large crystals of low magnesium

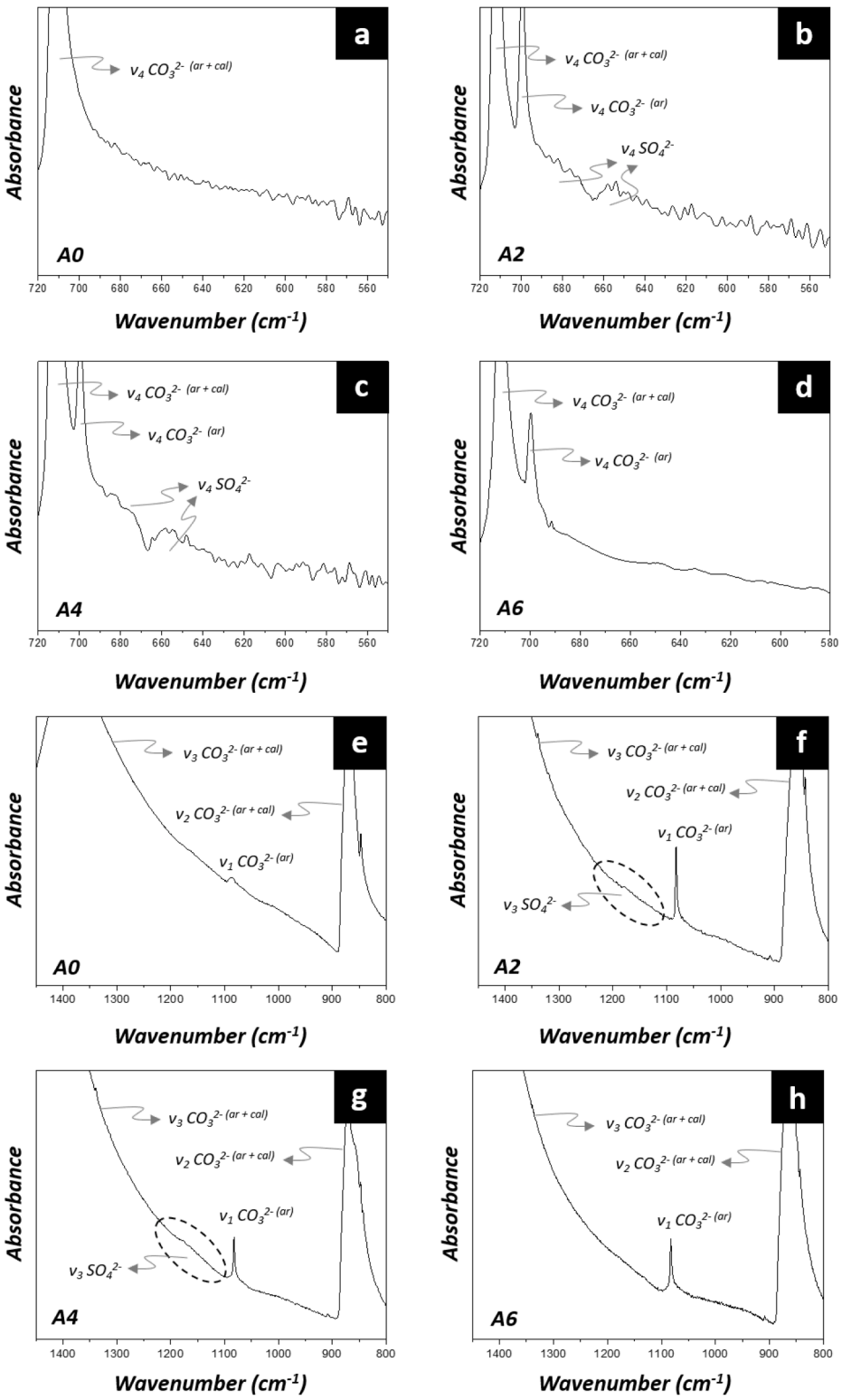

Fig. 9. FTIR spectra which shows a zoom of the spectra from Fig. 8 in the regions (a-d) 550 to 720 cm^{-1} and (e-h) 800 to 1450 cm^{-1}. In samples A2 and A4 there are bulges in the spectra that coincide with the regions where the v_3 and v_4 bands of the sulfate are found.

calcite (LMC). Once formed, the LMC crystals would protect the aragonite from further interaction with the diagenetic fluids, hindering the mass transfer between the bulk fluid and the reaction front and ultimately leading to a situation of partial equilibrium, where the fluid would be in equilibrium with the LMC rim but not with the aragonitic core. Sandberg and Hudson (1983) concluded that for the aragonite alteration to progress further, the LMC crystals should be remobilized first. This is unlikely to occur under common conditions in most diagenetic environments. We also must consider that the driving force for the recrystallization of calcites bearing impurities, like magnesium or sulfate, into pure calcite can be lower than that involved in the replacement of aragonite by calcite.

4.2. The role of sulfate in the transformation of aragonite to calcite

Our findings evidence that the presence of sulfate in the aqueous solution exerts a significant influence in the size, morphology and density of the calcite crystals formed on the aragonite dissolving surfaces. Thus, the average size of calcite crystals diminishes rapidly as sulfate concentration in solution increases (from over 40 μm when the solution lacks sulfate to below 10 μm for solutions featuring $[SO_4^{2-}]_{aq} \geq$ 5 mM; Figs. A8 and A9). Similarly, calcite crystal shape deviate from the cleavage rhombohedron morphology and calcite crystal density decreases with increasing sulfate concentration in the aqueous phase. It is interesting to note that while aragonite samples interacted with fluids containing $[SO_4^{2-}]_{aq} < 0.5$ show extensive fracturing, no fracturing is observed anymore in those aragonite samples interacted with solutions bearing $[SO_4^{2-}]_{aq} \geq 0.5$ mM. As stated above, once the thin boundary layer at the reaction front is in equilibrium with aragonite, it is also supersaturated with respect to calcite ($\beta \geq 1.14$ at 220 °C). This would be a supersaturation high enough to produce the necessary stress to open pre-existing 40 μm (and bigger) fractures. As can be seen in Fig. A8, in sulphate-poor systems there is a significant amount of crystals larger than this size. We can expect that these larger crystals growing within pre-existing fractures would be able to fill them and generate a stress enough to widen them and induce further fracturing of the aragonite substrate. On the other hand, the absence of fractures in aragonite samples interacted with fluids bearing $[SO_4^{2-}]_{aq} \geq 0.5$ mM may be attributed to a multi-fold influence of the sulfate oxyanions on calcite crystal features. It is widely accepted that small amounts of sulfate can incorporate into the crystal structure of calcite. Indeed, the infrared (IR) analysis of our altered aragonite crystals reveal minor vibrational bands corresponding to sulfate (Fig. 9). These bands are likely indicative of sulfate incorporation into the secondary calcite crystals. Busenberg and Plummer (1985) concluded that sulfate incorporation into calcite increases the solubility of this phase so that it surpasses that of pure aragonite when sulfate concentration in calcite is above 3.5 mol%. This interpretation has been later supported by the results of computer simulations, which point to the incorporation of increasing amounts of sulfate into calcite resulting in a progressive increase of calcite free energy and, as a result, solubility (Arroyo de Dompablo et al., 2015).

We expect that the interaction of aragonite with solutions with increasing amounts of sulfate will also result in the incorporation of higher amounts of sulfate in the calcite crystals formed on the aragonite surfaces. This incorporation will result in an increase of the solubility of the calcite crystals and, consequently, in a decrease of the aqueous solution supersaturation with respect to the growing phase. This reduction in supersaturation would make it increasingly difficult to produce the stresses necessary to open the pre-existing fractures on the aragonite substrates. Decreasing supersaturation in solutions with higher sulfate contents would also explain, the decreasing number of crystals that constitute the calcite overgrowths and also their increasingly smaller sizes. In the absence of fractures, the ICDP transformation of the primary phase into the secondary one is restricted to the most outermost region of the parent aragonite grains, which is occupied by a porosity-free, micrometric overgrowth. This overgrowth acts as a protective layer that armors the primary phase from further interaction with the fluid. Our results further reveal that as aragonite interacts with deionized water and calcium sulfate minerals (gypsum or anhydrite), the amount of sulfate ions released due to sulfate mineral dissolution is also high enough to preclude the aragonite to calcite transformation. Indeed, PHREEQ (Parkhurst and Appelo, 2013) simulations show that the concentration of sulfate in the aqueous solution in equilibrium with anhydrite and under the conditions of our experiments is 0.45 mM, very close to the threshold value of 0.5 mM.

The striking impact of sulfate in the size and density of secondary calcite crystals is likely the outcome of several factors. Atomic force microscopy (AFM) experiments have shown that even low concentrations of sulfate are sufficient to decrease the rate of calcite growth in sulfate-bearing fluids (Vavouraki et al., 2008). AFM measurements of the thickness of calcite monolayers are consistent with the incorporation of sulfate into the calcite lattice, with the extent of incorporation directly correlating with the sulfate content within the fluid. A inhibiting effect of calcite growth due to sulfate adsorption on calcite crystal surfaces can neither be discarded. The quantification of sulfate incorporation and/or absorption into overgrowing calcite crystals and a more comprehensive research into whether a correlation can be established between sulfate concentration in the bulk solution and calcite crystals features will have to be addressed in future works.

The presence of sulfate in the fluid also plays a key role in governing the morphology of the newly-formed calcite crystals. Crystals grown from solutions without sulfate exhibit the characteristic rhombohedral morphology of calcite abiogenic crystals. However, the habit of calcite crystals evolves with increasing sulfate concentration in the fluid so that they develop an increasingly prismatic habit. The impact of diverse ions on the habit of calcite has been extensively explored in the literature. We interpret that the elongation of calcite crystals arises from the reduction in surface energy associated with certain forms other than the rhombohedral one. This reduction stems from the selective adsorption of foreign ions onto these crystal faces (Titiloye et al., 1993; Aquilano et al., 2016). The prismatic, elongated habit of calcite crystals growing in sulfate -rich environments is consistent with observations made in experimental studies of $CaCO_3$ formation in the presence of dissolved sulfate and also in good agreement with the shapes of abiogenic calcite cements formed during the transformation of aragonitic fragments during experimental non-meteoritic diagenesis (Cuesta Mayorga et al., 2019; Hashim and Kaczmarek, 2022). The elongated habit of calcite crystals as well as the anisotropic development of equivalent faces can also relate to specific calcite-aragonite epitaxial relationships, whose study is beyond the scope of this study (Bruno et al., 2022).

5. Conclusions and implications for carbonate diagenesis

The findings of this work highlight the key role of sulfate in preventing the aragonite-calcite transformation through an ICDP reaction. Previous research (Perdikouri et al., 2011) showed that aragonite single crystals are transformed into calcite through the formation of an extensive network of fractures resulting from the crystallization pressure exerted by the calcite overgrowth on the aragonite substrate. These fractures allow fluid infiltration towards the unreacted aragonite surfaces, promoting further calcite precipitation and fracture formation. In this work we have shown that increasing amounts of sulfate in the fluid reduce the size (as well as the abundance) of the calcite crystals growing on aragonite surfaces. We interpret that the incorporation of sulfate into the crystal structure of calcite increases the solubility of this phase, which results in a lower supersaturation of the fluid with respect to this phase. The combined effect of reduced supersaturation and smaller crystal size leads to a decrease of the crystallization pressure exerted by the calcite overgrowth on the aragonite substrates, which fail to fracture. Consequently no transformation of aragonite into calcite occurs when the $[SO_4^{2-}]_{aq}$ overcomes a threshold value ($\geq$ 0.5 mM).

This study provides valuable insights for understanding the fate of aragonitic fragments during diagenesis. The transformation of aragonite into calcite, known in the literature by terms like inversion, stabilization, or neomorphism, represents one of the initial diagenetic processes undergone by carbonate sediments. While aragonite remains stable in a significant portion of today's ocean surfaces, which are supersaturated with respect to $CaCO_3$, it undergoes rapid dissolution and transformation into calcite in environments where the fluids are undersaturated with respect to aragonite but supersaturated with respect to calcite: i.e.: between the aragonite compensation depth (ACD) and the calcite compensation depth (CCD). Yet, the findings of this study highlight the key role that impurities in the diagenetic fluids play in influencing the survival of aragonite fragments. This work proves that moderate amounts of sulfate in the fluid are sufficient to hinder the

transformation of aragonite single crystals into calcite. In this study, we have found that sulfate alone can hinder this transition, without the need of any dissolved magnesium in the system. In natural settings, most diagenetic fluids commonly bear variable amounts of both sulfate and magnesium. The combined inhibitory effect of both ions may be synergistic in guaranteeing the preservation of aragonite, similarly as their influence is synergistic in promoting the metastable nucleation of aragonite above calcite (Bots et al., 2011; Goetschl et al., 2019). An in-depth study of this magnesium -sulfate, possibly synergistic, effect on the aragonite-calcite transformation will be the focus of further research. Modern-day seawater has an average sulfate concentration of 29 mM (Horita et al., 2002; Algeo et al., 2015). This concentration exceeds by a factor of 60 the sulfate concentration found as enough to hinder the aragonite-to-calcite transformation at the temperature (220 °C) and time framework of this study. Even in the geological periods characterized by lower sulfate levels in seawater, such as the Cretaceous or the Devonian (below 10 mM), $[SO_4^{2-}]_{aq}$ was significantly above the threshold revealed by our experiments. Notably, the experiments using naturally occurring Ca-sulfate minerals (gypsum or anhydrite) have shown that the dissolution of these mineral species commonly-found in sedimentary settings also yields fluids with sulfate concentrations high enough to hinder the transformation of aragonite into calcite, at least within the time framework of this study. The latter results show that the pre-existing mineral phases may strongly affect the ageing of calcium carbonate mineral phases. Despite the common concurrence of carbonates and other minerals like clays, silicates and sulfates in natural settings, this influence is poorly understood and additional research will have to be conducted in future (Molnár et al., 2021)

Sulfate not only impacts the stability of the aragonitic fragments, preventing their extensive transformation into calcite. It also significantly influences the morphology of the secondary calcite crystals. Thus, calcite crystals grown in fluids bearing high concentrations of sulfate exhibit elongated prismatic shapes, a departure from the rhombohedral morphologies which are dominant in calcite crystals growing in sulfate-free fluids. Recent studies have suggested that the morphology of abiogenic calcite crystals replacing aragonitic fragments in limestones could serve as a proxy to trace the diagenetic history of the rock (Hashim and Kaczmarek, 2022). The rhombohedral microcrystalline crystals found in many Phanerozoic limestones are proposed to form through the mineralogical stabilization of metastable $CaCO_3$ precursors during meteoric diagenesis. In contrast, calcite crystals formed under conditions akin to marine diagenesis would display non-rhombohedral morphologies. The results of this study appear to support this hypothesis. Finally, this study highlights the significant disparity in the mechanism and kinetics of transformation of aragonite single crystals compared to aragonitic biominerals (Perdikouri et al., 2011; Forjanes et al., 2022). The conversion of aragonite single crystals involves the development of an extensive fracture network, triggered by the increase in molar volume associated to the aragonite into calcite transformation. Contrarily, biominerals undergo replacement by abiogenic calcite thanks to the development of a network of secondary porosity as biopolymer degradation takes place. This, together to the composite nature and enhanced mechanical properties of biominerals, prevents the formation of fractures. The substantial variations in the mechanism and pace of the replacement process amongst diverse biogenic aragonitic microstructures and abiogenic aragonitic materials underscore the need for further research to better comprehend the controlling mechanisms of this transformation (Casella et al., 2018; Pederson et al., 2020)

CRediT authorship contribution statement

Pablo Forjanes: Writing – review & editing, Writing – original draft, Visualization, Software, Methodology, Investigation, Formal analysis, Data curation, Conceptualization. **José Manuel Astilleros:** Writing – review & editing, Validation, Supervision, Resources, Project administration, Funding acquisition. **Lurdes Fernández-Díaz:** Writing – review & editing, Validation, Supervision, Resources, Project administration, Funding acquisition.

Declaration of competing interest

The authors declare that they have no known competing financial interests or personal relationships that could have appeared to influence the work reported in this paper.

Data availability

Data will be made available on request.

Acknowledgments

This work has been funded through the project PID2021–125467NB-I00 of the Spanish Ministry of Science, Innovation and Universities and through a Helmholtz Recruitment Initiative (grant number I-044–16–01) awarded to Liane G. Benning. Pablo Forjanes acknowledges the support from a FPU predoctoral contract (Formación del Profesorado Universitario - FPU17/01689) from the Spanish Ministry of Universities. We thank Liane G. Benning for the comments and suggestions that have helped to improve the manuscript. We also thank Ana Vicente, from the Centro Nacional de Microscopía Electrónica (CNME-UCM) and Chiara Bahl, from the GeoForschungsZentrum (GFZ-Potsdam) for their help in obtaining the microscopy images. We thank two anonymous reviewers for their insightful comments which have helped to improve the manuscript.

Supplementary materials

Supplementary material associated with this article can be found, in the online version, at doi:10.1016/j.epsl.2024.118771.

References

Algeo, T.J., Luo, G.M., Song, H.Y., Lyons, T.W., Canfield, D.E., 2015. Reconstruction of secular variation in seawater sulfate concentrations. Biogeosciences 12, 2131–2151. https://doi.org/10.5194/bg-12-2131-2015.

Aquilano, D., Otálora, F., Pastero, L., García-Ruiz, J.M., 2016. Three study cases of growth morphology in minerals: halite, calcite and gypsum. Prog. Cryst. Growth Charact. Mater. 62, 227–251. https://doi.org/10.1016/j.pcrysgrow.2016.04.012. Special Issue: Recent Progress On Fundamentals and Applications of Crystal Growth; Proceedings of the 16th International Summer School on Crystal Growth (ISSCG-16).

Arroyo de Dompablo, M.E.A., Fernández-González A., M., Fernández-Díaz, L., 2015. Computational investigation of the influence of tetrahedral oxoanions (sulphate, selenate and chromate) on the stability of calcium carbonate polymorphs. RSC Adv. 5, 59845–59852. https://doi.org/10.1039/C5RA08574H.

Astilleros, J.M., Fernández-Díaz, L., Putnis, A., 2010. The role of magnesium in the growth of calcite: an AFM study. Chem. Geol. 271, 52–58. https://doi.org/10.1016/j.chemgeo.2009.12.011.

Bischoff, J.L., Fyfe, W.S., 1968. Catalysis, inhibition, and the calcite-aragonite problem; [Part] 1, The aragonite-calcite transformation. Am. J. Sci. 266, 65–79. https://doi.org/10.2475/ajs.266.2.65.

Boon, M., Rickard, W.D.A., Rohl, A.L., Jones, F., 2020. Stabilization of Aragonite: role of Mg^{2+} and other impurity ions. Cryst. Growth Des. 20, 5006–5017. https://doi.org/10.1021/acs.cgd.0c00152.

Bots, P., Benning, L.G., Rickaby, R.E.M., Shaw, S., 2011. The role of SO_4 in the switch from calcite to aragonite seas. Geology 39, 331–334. https://doi.org/10.1130/G31619.1.

Brown, W.H., Fyfe, W.S., Turner, F.J., 1962. Aragonite in California Glaucophane Schists, and the kinetics of the aragonite—calcite transformation. J. Petrol. 3, 566–582. https://doi.org/10.1093/petrology/3.3.566.

Bruno, M., Prencipe, M., Aquilano, D., Cotellucci, A., Ghignone, S., Németh, P., 2022. Calcite/Aragonite Epitaxy: a computational study for understanding mollusk shell formation. J. Phys. Chem. C 126, 6472–6481. https://doi.org/10.1021/acs.jpcc.2c00785.

Busenberg, E., Niel Plummer, L., 1985. Kinetic and thermodynamic factors controlling the distribution of SO_3^{2-} and Na^+ in calcites and selected aragonites. Geochim. Cosmochim. Acta 49, 713–725. https://doi.org/10.1016/0016-7037(85)90166-8.

Carlson, W.D., 1983. Chapter 6. The polymorphs of $CaCO_3$ and the aragonite-calcite transformation. Carbonates: Mineralogy and Chemistry. Reviews in Mineralogy. De Gruyter, pp. 191–226. https://doi.org/10.1515/9781501508134-010.

Casella, L.A., Griesshaber, E., Yin, X., Ziegler, A., Mavromatis, V., Müller, D., Ritter, A.C., Hippler, D., Harper, E.M., Dietzel, M., Immenhauser, A., Schöne, B.R., Angiolini, L., Schmahl, W.W., 2017. Experimental diagenesis: insights into aragonite to calcite transformation of *Arctica islandica* shells by hydrothermal treatment. Biogeosciences 14, 1461–1492. https://doi.org/10.5194/bg-14-1461-2017.

Casella, L.A., He, S., Griesshaber, E., Fernández-Díaz, L., Greiner, M., Harper, E.M., Jackson, D.J., Ziegler, A., Mavromatis, V., Dietzel, M., Eisenhauer, A., Veintemillas-Verdaguer, S., Brand, U., Schmahl, W.W., 2018. Hydrothermal alteration of aragonitic biocarbonates: assessment of micro- and nanostructural dissolution–reprecipitation and constraints of diagenetic overprint from quantitative statistical grain-area analysis. Biogeosciences 15, 7451–7484. https://doi.org/10.5194/bg-15-7451-2018.

Choi, S., Kim, N.H., Kim, H.I., Kweon, J.J., Lee, S.K., Zhang, S., Varricchio, D.J., 2022. Preservation of aragonite in Late Cretaceous (Campanian) turtle eggshell. Palaeogeogr. Palaeoclimatol. Palaeoecol. 585, 110741 https://doi.org/10.1016/j.palaeo.2021.110741.

Cuesta Mayorga, I., Astilleros, J.M., Fernández-Díaz, L., 2019. Precipitation of $CaCO_3$ Polymorphs from aqueous solutions: the role of pH and Sulphate groups. Minerals 9, 178. https://doi.org/10.3390/min9030178.

Davis, K.J., Dove, P.M., De Yoreo, J.J., 2000. The role of Mg^{2+} as an impurity in calcite growth. Science 290, 1134–1137. https://doi.org/10.1126/science.290.5494.1134.

De Villiers, J.P.R., 1971. Crystal structures of aragonite, strontianite, and witherite. Am. Mineral. 56, 758–767.

De Yoreo, J.J., Vekilov, P.G., 2003. Principles of crystal nucleation and growth. Rev. Mineral. Geochem. 54, 57–93. https://doi.org/10.2113/0540057.

Ernst, W.G., 1988. Tectonic history of subduction zones inferred from retrograde blueschist P-T paths. Geology 16, 1081–1084. https://doi.org/10.1130/0091-7613(1988)016<1081:THOSZI>2.3.CO;2.

Fernández-Díaz, L., Fernández-González, Á., Prieto, M., 2010. The role of sulfate groups in controlling $CaCO_3$ polymorphism. Geochim. Cosmochim. Acta 74, 6064–6076. https://doi.org/10.1016/j.gca.2010.08.010.

Fernandez-Diaz, L., Putnis, A., Prieto, M., Putnis, C.V., 1996. The role of magnesium in the crystallization of calcite and aragonite in a porous medium. J. Sediment. Res. 66, 482–491. https://doi.org/10.1306/D4268388-2B26-11D7-8648000102C1865D.

Forjanes, P., Simonet Roda, M., Greiner, M., Griesshaber, E., Lagos, N.A., Veintemillas-Verdaguer, S., Astilleros, J.M., Fernández-Díaz, L., Schmahl, W.W., 2022. Experimental burial diagenesis of aragonitic biocarbonates: from organic matter loss to abiogenic calcite formation. Biogeosciences 19, 3791–3823. https://doi.org/10.5194/bg-19-3791-2022.

Frisia, S., Borsato, A., Fairchild, I.J., mcdermott, F., Selmo, E.M., 2002. Aragonite-calcite relationships in Speleothems (Grotte De Clamouse, France): environment, fabrics, and carbonate geochemistry. J. Sediment. Res. 72, 687–699. https://doi.org/10.1306/020702720687.

Goetschl, K.E., Purgstaller, B., Dietzel, M., Mavromatis, V., 2019. Effect of sulfate on magnesium incorporation in low-magnesium calcite. Geochim. Cosmochim. Acta 265, 505–519. https://doi.org/10.1016/j.gca.2019.07.024.

Hardie, L.A., 1996. Secular variation in seawater chemistry: an explanation for the coupled secular variation in the mineralogies of marine limestones and potash evaporites over the past 600 m.y. Geology 24, 279–283. https://doi.org/10.1130/0091-7613(1996)024<0279:SVISCA>2.3.CO;2.

Hashim, M.S., Kaczmarek, S.E., 2022. Rhombic calcite microcrystals as a textural proxy for meteoric diagenesis. Sci. Rep. 12, 213. https://doi.org/10.1038/s41598-021-04219-2.

Hashim, M.S., Kaczmarek, S.E., 2021. The transformation of aragonite to calcite in the presence of magnesium: implications for marine diagenesis. Earth Planet. Sci. Lett. 574, 117166 https://doi.org/10.1016/j.epsl.2021.117166.

Hashim, M.S., Kaczmarek, S.E., 2019. A review of the nature and origin of limestone microporosity. Mar. Pet. Geol. 107, 527–554. https://doi.org/10.1016/j.marpetgeo.2019.03.037.

Herrero, M.J., Marfil, R., Escavy, J.I., Scherer, M., Arroyo, X., Martín-Crespo, T., López de Andrés, S., 2020. Hydrothermal activity within a sedimentary succession: aragonites as indicators of Mesozoic Rifting (Iberian Basin, Spain). Int. Geol. Rev. 62, 94–112. https://doi.org/10.1080/00206814.2019.1636317.

Horita, J., Zimmermann, H., Holland, H.D., 2002. Chemical evolution of seawater during the Phanerozoic: implications from the record of marine evaporites. Geochim. Cosmochim. Acta 66, 3733–3756. https://doi.org/10.1016/S0016-7037(01)00884-5.

Idrissi, H., Bollinger, C., Boioli, F., Schryvers, D., Cordier, P., 2016. Low-temperature plasticity of olivine revisited with in situ TEM nanomechanical testing. Sci. Adv. 2, e1501671 https://doi.org/10.1126/sciadv.1501671.

Jamtveit, B., Putnis, C.V., Malthe-Sørenssen, A., 2009. Reaction induced fracturing during replacement processes. Contrib. Mineral. Petrol. 157, 127–133. https://doi.org/10.1007/s00410-008-0324-y.

Julia, M., Putnis, C.V., King, H.E., Renard, F., 2023. Coupled dissolution-precipitation and growth processes on calcite, aragonite, and Carrara marble exposed to cadmium-rich aqueous solutions. Chem. Geol. 621, 121364 https://doi.org/10.1016/j.chemgeo.2023.121364.

Katti, D.R., Katti, K.S., 2001. Modeling microarchitecture and mechanical behavior of nacre using 3D finite element techniques Part I Elastic properties. J. Mater. Sci. 36, 1411–1417. https://doi.org/10.1023/A:1017528209162.

Katz, A., 1973. The interaction of magnesium with calcite during crystal growth at 25–90°C and one atmosphere. Geochim. Cosmochim. Acta 37, 1563–1586. https://doi.org/10.1016/0016-7037(73)90091-4.

Lafay, R., Montes-Hernandez, G., Renard, F., Vonlanthen, P., 2018. Intracrystalline reaction-induced cracking in olivine evidenced by hydration and carbonation experiments. Minerals 8, 412. https://doi.org/10.3390/min8090412.

Lew, A.J., Stifler, C.A., Tits, A., Schmidt, C.A., Scholl, A., Cantamessa, A., Müller, L., Delaunois, Y., Compère, P., Ruffoni, D., Buehler, M.J., Gilbert, P.U.P.A., 2023. A molecular-scale understanding of misorientation toughening in corals and seashells. Adv. Mater. 35, 2300373 https://doi.org/10.1002/adma.202300373.

Lippmann, F., 1973. Crystal chemistry of sedimentary carbonate minerals. Lippmann, F. (Ed.). Sedimentary Carbonate Minerals, Minerals, Rocks and Inorganic Materials. Springer, Berlin, Heidelberg, pp. 5–96. https://doi.org/10.1007/978-3-642-65474-9_2.

Markgraf, S.A., Reeder, R.J., 1985. High-temperature structure refinements of calcite and magnesite. Am. Mineral. 70, 590–600.

Meyers, M.A., Lin, A.Y.M., Chen, P.Y., Muyco, J., 2008. Mechanical strength of abalone nacre: role of the soft organic layer. J. Mech. Behav. Biomed. Mater. 1, 76–85. https://doi.org/10.1016/j.jmbbm.2007.03.001.

Molnár, Z., Pekker, P., Dódony, I., Pósfai, M., 2021. Clay minerals affect calcium (magnesium) carbonate precipitation and aging. Earth Planet. Sci. Lett. 567, 116971 https://doi.org/10.1016/j.epsl.2021.116971.

Monasterio-Guillot, L., Fernandez-Martinez, A., Ruiz-Agudo, E., Rodriguez-Navarro, C., 2021. Carbonation of calcium-magnesium pyroxenes: physical-chemical controls and effects of reaction-driven fracturing. Geochim. Cosmochim. Acta 304, 258–280. https://doi.org/10.1016/j.gca.2021.02.016.

Morse, J.W., Arvidson, R.S., Lüttge, A., 2007. Calcium carbonate formation and dissolution. Chem. Rev. 107, 342–381. https://doi.org/10.1021/cr050358j.

Mucci, A., 1986. Growth kinetics and composition of magnesian calcite overgrowths precipitated from seawater: quantitative influence of orthophosphate ions. Geochim. Cosmochim. Acta 50, 2255–2265. https://doi.org/10.1016/0016-7037(86)90080-3.

Nielsen, L.C., De Yoreo, J.J., DePaolo, D.J., 2013. General model for calcite growth kinetics in the presence of impurity ions. Geochim. Cosmochim. Acta 115, 100–114. https://doi.org/10.1016/j.gca.2013.04.001.

Nielsen, M.R., Sand, K.K., Rodriguez-Blanco, J.D., Bovet, N., Generosi, J., Dalby, K.N., Stipp, S.L.S., 2016. Inhibition of calcite growth: combined effects of Mg2+ and SO42. Cryst. Growth Des. 16, 6199–6207. https://doi.org/10.1021/acs.cgd.6b00536.

Parkhurst, D.L.; Appelo, C.A.J.; 2013. Description of input and examples for PHREEQC version 3–A computer program for speciation, batch-reaction, one- dimensional transport, and inverse geochemical calculations. U.S. Geological Survey Techniques and Methods, Book 6, chap. A43.

Pederson, C.L., Mavromatis, V., Dietzel, M., Rollion-Bard, C., Breitenbach, S.F.M., Yu, D., Nehrke, G., Immenhauser, A., 2020. Variation in the diagenetic response of aragonite archives to hydrothermal alteration. Sediment. Geol. 406, 105716 https://doi.org/10.1016/j.sedgeo.2020.105716.

Perdikouri, C., Kasioptas, A., Geisler, T., Schmidt, B.C., Putnis, A., 2011. Experimental study of the aragonite to calcite transition in aqueous solution. Geochim. Cosmochim. Acta 75, 6211–6224. https://doi.org/10.1016/j.gca.2011.07.045.

Plummer, L.N., Busenberg, E., 1982. The solubilities of calcite, aragonite and vaterite in CO_2-H_2O solutions between 0 and 90 °C, and an evaluation of the aqueous model for the system $CaCO_3$-CO_2-H_2O. Geochim. Cosmochim. Acta 46, 1011–1040. https://doi.org/10.1016/0016-7037(82)90056-4.

Plümper, O., Røyne, A., Magrasó, A., Jamtveit, B., 2012. The interface-scale mechanism of reaction-induced fracturing during serpentinization. Geology 40, 1103–1106. https://doi.org/10.1130/G33390.1.

Putnis, A., 2009. Mineral replacement reactions. Rev. Mineral. Geochem. 70, 87–124. https://doi.org/10.2138/rmg.2009.70.3.

Putnis, A., Putnis, C.V., 2007. The mechanism of reequilibration of solids in the presence of a fluid phase. J. Solid State Chem. 180, 1783–1786. https://doi.org/10.1016/j.jssc.2007.03.023.

Putnis, C.V., Putnis, A., 2022. A mechanism of ion exchange by interface-coupled dissolution-precipitation in the presence of an aqueous fluid. J. Cryst. Growth 600, 126840. https://doi.org/10.1016/j.jcrysgro.2022.126840.

Qian, G., Brugger, J., Skinner, W.M., Chen, G., Pring, A., 2010. An experimental study of the mechanism of the replacement of magnetite by pyrite up to 300°C. Geochim. Cosmochim. Acta 74, 5610–5630. https://doi.org/10.1016/j.gca.2010.06.035.

Qian, G., Xia, F., Brugger, J., Skinner, W.M., Bei, J., Chen, G., Pring, A., 2011. Replacement of pyrrhotite by pyrite and marcasite under hydrothermal conditions up to 220°C: an experimental study of reaction textures and mechanisms. Am. Mineral. 96, 1878–1893. https://doi.org/10.2138/am.2011.3691.

Ross, S.D., 1974. Sulphates and other oxy-anions of group VI. Farmer, V.C. (Ed.). The Infrared Spectra of Minerals. Mineralogical Society of Great Britain and Ireland. https://doi.org/10.1180/mono-4.18, p. 0.

Røyne, A., Jamtveit, B., Mathiesen, J., Malthe-Sørenssen, A., 2008. Controls on rock weathering rates by reaction-induced hierarchical fracturing. Earth Planet. Sci. Lett. 275, 364–369. https://doi.org/10.1016/j.epsl.2008.08.035.

Ruiz-Agudo, E., Putnis, C.V., Putnis, A., 2014. Coupled dissolution and precipitation at mineral–fluid interfaces. Chem. Geol. 383, 132–146. https://doi.org/10.1016/j.chemgeo.2014.06.007.

Sandberg, P.A., Hudson, J.D., 1983. Aragonite relic preservation in Jurassic calcite-replaced bivalves. Sedimentology 30, 879–892. https://doi.org/10.1111/j.1365-3091.1983.tb00716.x.

Scherer, G.W., 1999. Crystallization in pores. Cem. Concr. Res. 29, 1347–1358. https://doi.org/10.1016/S0008-8846(99)00002-2.

Schiro, M., Ruiz-Agudo, E., Rodriguez-Navarro, C., 2012. Damage mechanisms of porous materials due to in-pore salt crystallization. Phys. Rev. Lett. 109, 265503 https://doi.org/10.1103/PhysRevLett.109.265503.

Staudt, W.J., Reeder, R.J., Schoonen, M.A.A., 1994. Surface structural controls on compositional zoning of SO_4^{2-} and SeO_4^{2-} in synthetic calcite single crystals. Geochim. Cosmochim. Acta 58, 2087–2098. https://doi.org/10.1016/0016-7037(94)90287-9.

Steiger, M., 2005. Crystal growth in porous materials—I: the crystallization pressure of large crystals. J. Cryst. Growth 282, 455–469. https://doi.org/10.1016/j.jcrysgro.2005.05.007.

Sun, W., Jayaraman, S., Chen, W., Persson, K.A., Ceder, G., 2015. Nucleation of metastable aragonite CaCO3 in seawater. Proc. Natl. Acad. Sci. U. S. A. 112, 3199–3204. https://doi.org/10.1073/pnas.1423898112.

Titiloye, J.O., Parker, S.C., Mann, S., 1993. Atomistic simulation of calcite surfaces and the influence of growth additives on their morphology. J. Cryst. Growth 131, 533–545. https://doi.org/10.1016/0022-0248(93)90205-B.

Toffolo, M.B., Regev, L., Dubernet, S., Lefrais, Y., Boaretto, E., 2019. FTIR-based crystallinity assessment of aragonite–calcite mixtures in archaeological lime binders altered by diagenesis. Minerals 9, 121. https://doi.org/10.3390/min9020121.

Turchyn, A.V., Bradbury, H.J., Walker, K., Sun, X., 2021. Controls on the precipitation of carbonate minerals within marine sediments. Front. Earth Sci. 9.

Vagenas, N.V., Gatsouli, A., Kontoyannis, C.G., 2003. Quantitative analysis of synthetic calcium carbonate polymorphs using FT-IR spectroscopy. Talanta 59, 831–836. https://doi.org/10.1016/S0039-9140(02)00638-0.

Vavouraki, A.I., Putnis, C.V., Putnis, A., Koutsoukos, P.G., 2008. An atomic force microscopy study of the growth of calcite in the presence of sodium sulfate. Chem. Geol. 253, 243–251. https://doi.org/10.1016/j.chemgeo.2008.05.013.

Zhao, J., Brugger, J., Chen, G., Ngothai, Y., Pring, A., 2014. Experimental study of the formation of chalcopyrite and bornite via the sulfidation of hematite: mineral replacements with a large volume increase. Am. Mineral. 99, 343–354. https://doi.org/10.2138/am.2014.4628.